Journal of Engineering Research and Reports

Volume 25, Issue 1, Page 11-40, 2023; Article no.JERR.98767
ISSN: 2582-2926

Monitoring Land Changes Using Remote Sensing Methods and Spatial Information System in the Area of Kahrizak Waste Disposal Center

Vahid Hatamzadeh [a*], Sara Vahidi [a], Shokofeh Karimi [a], Afshin Afshinfar [a] and Paniz Nouri [a]

[a] South Tehran Azad University, Iran.

Authors' contributions

This work was carried out in collaboration among all authors. All authors read and approved the final manuscript.

Article Information

DOI: 10.9734/JERR/2023/v25i1867

Open Peer Review History:
This journal follows the Advanced Open Peer Review policy. Identity of the Reviewers, Editor(s) and additional Reviewers, peer review comments, different versions of the manuscript, comments of the editors, etc are available here: https://www.sdiarticle5.com/review-history/98767

Original Research Article

Received: 18/02/2023
Accepted: 20/04/2023
Published: 27/04/2023

ABSTRACT

With more than 50 years of proximity to Tehran metropolis, the Kehrizak waste center has had destructive effects on the environment with the development of Tehran and the significant increase in waste production, including the change of land use units that are always affected by natural events, human actions, social issues and Economic. In this research, using Landsat 8 satellite images and remote sensing technique, the land use changes of Kahrizek waste center in thematic maps that are more accessible to users. Five vegetation indices NDVI, EVI, SAVI, LAI and VCI and six supervised classifications are investigated. Several methods were evaluated, parameters of overall accuracy and kappa coefficient. For this research, 4 classes of soil, water, building (urban area) and agricultural land were selected, and the results showed that the maximum likelihood classification method was the best method with an overall accuracy of 90.99% and a kappa coefficient of 0.85 and high similarity. Then, using the maximum likelihood classification method as

**Corresponding author: Email: vahid4251@yahoo.com;*

the most accurate method, a user map was prepared from all images from 2011 to 2022. After calculating the area of the floors, the results showed that the area of the building floor increased by 71% and the area of the agricultural land floor decreased by 80%.

Keywords: Remote sensing; Kahrizak landfill; landsat8 satellite images; classification methods.

1. INTRODUCTION

In the recent decades the growth of urbanization and excessive waste production caused improving area around the cities to become or expand into landfills and destroy the agricultural lands around them. As a result, it is necessary to evaluate the process changes in the city and to be aware of the change's pattern and apply it in the planning and management of big cities. 5The new technology of remote sensing, in addition to its unique features such as wide vision and repeated coverage, high speed of information transfer, has made this science more widely used in recent years. Using satellite images in this regard is very cost-effective and useful. Using common and traditional methods of land measurement requires a lot of time and cost, and it is not possible to do it even in some inaccessible areas. So far, no studies have been done by satellite images and remote sensing methods to monitor land use changes in the Kahrizak waste center, On the other hand, two or more images have been used in the studies to monitor land use changes, but in this research, one image has been considered for each year so that land use changes can be full monitored. Also, for this research, not only one remote sensing method was used to monitor land use changes, but different methods including classification methods and vegetation indicators were used to monitor land use changes in Kahrizak Waste Center. Classification of images is one of the important techniques in the interpretation of images, which is widely used in this study of land changes. The important issue is to determine the classification method with appropriate accuracy for the desired satellite images. The use of satellite images due to its special features such as wide visibility and low cost, using different parts of the electromagnetic spectrum to record the characteristics of phenomena, short return period, the possibility of automatic analysis, faster investigation and also providing the possibility of monitoring the area, have a particular importance [1]. In 2019, Hisham Abdul Mansef et al. used the combination of remote sensing, geographic information system and hierarchical analysis process to select a hazardous waste landfill site. The area studied in this research was the hazardous industrial wastes of the Suez Canal in Egypt. To implement the AHP model, they used the parameters set in the Basel Convention on Hazardous Waste, which was established in 1992. These parameters included social, economic, environmental, geological, hydrological and geomorphological parameters. Using the AHP method and the mentioned parameters, two suitable places for hazardous waste disposal were identified [2]. Remote sensing data with features such as repeated imaging in short time intervals, the vastness of the land cover surface taken by the sensors, suitable spectral and spatial resolution of the data provide a suitable tool for investigating land cover changes. Today, progress in remote sensing techniques has provided considerable opportunities and successes to observe and manage the rapid growth of cities. In the field of determining land use and land cover, many studies have been conducted in the world and the use of satellite data such as Landsat, Spot and IRS in preparing maps has been approved by many experts. Several researches in this field have done. aljenaid et al detected land use and land cover using GIS and remote sensing technique in Bahrain over 1986-2020.they used multi spectral and multi temporal land sat satellite imagery. They classified images using maximum likelihood algorithm to generate the seven LULC maps [3]. In 2022, Bilal Aslam et al. identified and ranked landfill sites for urban solid waste in Faisalabad city in Pakistan using the combination of remote sensing and GIS. In this study, they used Landsat 8 images and vegetation indices NDVI, NDWI and NDBI and 3 parameters of population, roads and water areas. The generated suitability map for landfill is divided into 5sections: very good, good, average, poor and very poor [4]. In 2022, Abdullah Ezzeddin Karabulut and colleagues used the combination of remote sensing and GIS and AHP method to locate the landfill in Sanliurfa city in Turkey. For this research, they used the images of Landsat 5 in 1989 and Landsat 8 in 2019 to produce a land use map and NDVI vegetation index. Using digital elevation model data, they produced

height, slope and slope direction maps. Then, by weighting the maps and implementing the AHP model in the GIS environment, they concluded that 13.51% of the area is suitable for landfilling [5]. Clarifying and predicting the changes in land covering and urban growth are keys to present the holistic and principled views on more efficient management of environmental resources, protection of suburban lands and adoption of long-term policies to minimize the impacts of urban development on the environment and even to appreciate the potential impacts on socioeconomic resources as well as people [6]. In 2022, Nima Karimi and colleagues used satellite images to identify the areas of landfill without permission in the Saskatchewan region, located north of Saskatoon in Canada. For this research, they used Landsat 8 images to produce land surface temperature and MSAVI vegetation index and vector data of railways and highways. In this research, by weighting the layers and using the fuzzy method, unlicensed landfill areas were discovered and favorable areas for landfilling were also located [7]. In 2022, Ike Felix et al used remote sensing and GIS techniques to identify suitable sites for solid waste disposal in the city of Aba, located in the southeast of Nigeria. For this research, they used Landsat 8 image, SRTM data, GPS coordinates, geological map, soil map, and land use map to produce a suitability map of areas for landfilling. The results showed that the most suitable potential areas for solid waste landfill sites are located about 5000 meters west of Ariaria market and 10000 meters southeast of Umo Mba in Aba city [8]. Kumar and Singh studied on geospatial application in land use land cover detection in developed region. They used Landsat 2,3,5,7 and 8 image for the years 1975-2020 for central Haryana, India. They used unsupervised classification to classify the images in eight classes .the year 1975 considered as the base year for change detection analysis. Their results showed an increasing trend for the land use classes of built-up, water body and agricultural land without water logging between 1975 and 2020.also land use classes of agriculture with water logging, open water logged area vegetation and fallow land decreased during the same period. The most achievement of their paper is the human activity had a great impact on land-cover land-changes in the developed area [9]. Gun et al 2020 studied a CD and classification algorithm for urban expansion processes in Tianjin (coastal city in china) based on Landsat time series from 1985 to 2019.they applied the C-factor approach with the Ross Thick-LiSparse-R model to correct the bidirectional reflectance distribution function (BRDF) effect for each Landsat image and calculated a spatial line density feature to improving the CD and the classification [10]. The purpose of this study is to monitor land use changes in the area of Kahrizak waste disposal center using remote sensing and spatial information system. So far, no studies have been done by satellite images and remote sensing methods to monitor land use changes in the Kahrizak waste center, if the wastes of the metropolis of Tehran are buried in the Kahrizak waste center. On the other hand, two or more images have been used in the studies to monitor land use changes, but in this research, one image has been considered for each year so that land use changes can be monitored and compare several methods in classification and remote sensing indices checked out. During this research work, according to the above classification, the comparison of different methods was done, and also the drought indicators from the point of view make the desired study more complete, it is noteworthy that 3000 points were taken in the form of ground data and GPS to confirm the information obtained. It distinguishes the work from other researches.

1.1 Study Area

The Kehrizak landfill center is located in the south of Kehrizak and at the beginning of the Tehran-Qom road. Area of this center is about 1400 hectares and it has been accepting the waste of Tehran since1956. The studied area is located at the longitude of $51°:23'$ and the latitude $35°:34'$. In order to monitor land cover and changes in the Kahrizak landfill, a buffer of 10 km from the landfill has been considered. The location of the study area is shown in the Fig. 1.

2. MATERIALS AND METHODS

After downloading landsat8 (OLI sensor)'s images with 30meter spatial resolution, second step is Preprocessing of satellite images. Pre-processing of images includes making corrections on them. The products provided by Landsat have different levels of corrections. For this research, level 1 ground corrected images have been used. In the corrected images of level 1(Level1 Terrain corrected), Landsat images are very large images and according to the purpose of the research to monitor land use changes in

the area of the Kahrizak landfill, a buffer of 10 km from the landfill has been considered. In the area considered for study, a part of Behesht Zahra lands has been observed, precise geometrical corrections have been made using ground control points and digital earth model. For proving geometric accuracy the ground control points used in this level are obtained from the GLS2000 dataset and the digital elevation model of the earth through sources such as GTOPO30, CDED NED, SRTM. At this level, other corrections are made due to gauge errors, satellite errors, and ground errors [12],after that radiometric correction have been applied, Radiometric corrections are performed to improve the radiometric quality of the images, increase the resolution and, as a result, increase the amount of information that can be extracted from the images. Radiometric corrections have been done in the following two steps:

1. Conversion of numerical pixel values in each image to radiation flux density
2. Converting radiant density to surface reflectance using the FLAASH method

Fig. 2 depicts the fellow-chart of research process.

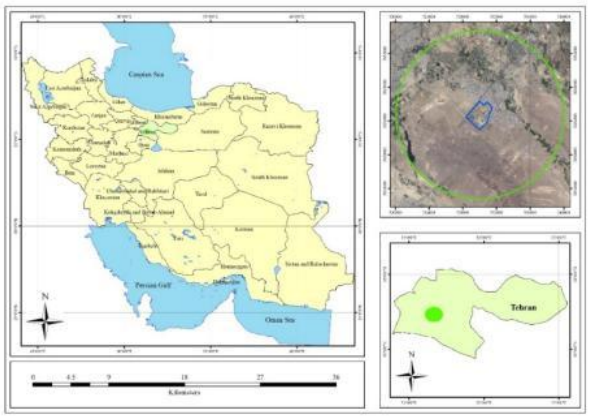

Fig. 1. The location of study area [11]

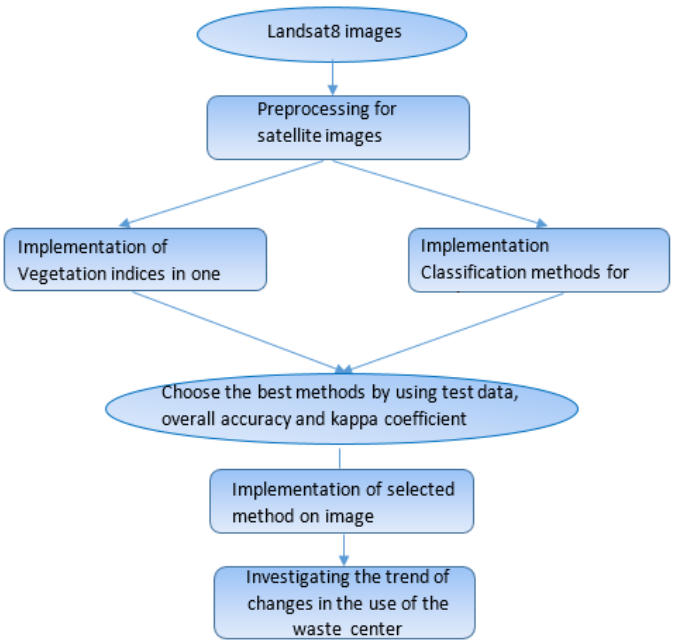

Fig. 2. Fellow chart of research processing

Some of processing in this research had been done by ENVI 5.6 (The Environment for Visualizing Images) for computing indices (NDVI, EVI, SAVI, LAI and VCI) and spatial analysis and providing Land use maps for every year in the study area, done by ArcGIS software.

2.1 Improving Spatial Resolution

In this process, by using different satellite images with different spatial resolutions, the data integration process can be applied to improve the quality and quantity of the images. There are various methods of performing fusion, which include:

- Methods based on cell processing
- Methods based on complications
- Statistical methods

The results of merging data have more spatial resolution, appropriate accuracy and have a valuable visual quality for interpretation also it can provide the possibility of targeted processing of multi-temporal, multi-sensor and multi-spectral images. Classification methods can be improve by spatial resolution increment [24].

2.2 Implementation of Classification Methods

Image classification methods are divided into 3 groups: supervised classification methods, unsupervised classification methods, and object-oriented classification methods [13].

2.2.1 Supervised classification methods

In this method of classification, there is a need for previous information and knowledge of the phenomena related to the data, and a number of pixels are introduced to the software as identifiers (training examples), then the software classifies the rest of the pixels according to specific instructions. In the following, some supervised classification methods are introduced.

2.2.1.1 Classification of the minimum distance from the average

The mean of all classes that have been separated from each other using the method of determining educational areas is determined, and then the Euclidean distance of the reflection of each pixel is calculated from the mean of all classes. Each pixel belongs to a class that has the smallest distance to the mean of that class. This type of classifier is mathematically simple and computationally efficient, but it tries to divide the multispectral space without using information such as variances.

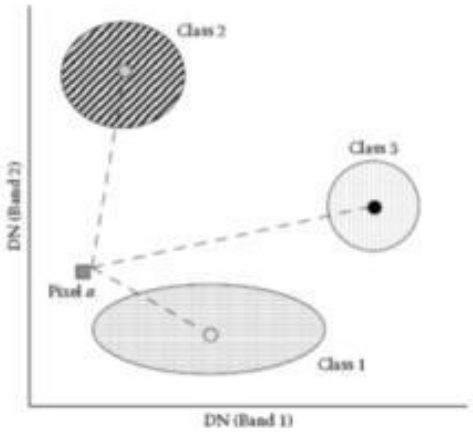

Fig. 3. Schematic visualization of the minimum distance from the mean classifier [13]

2.2.1.2 Mahalanobis distance classification

In this algorithm assumed that the histogram of the bands have a normal distribution. The use of variance and covariance in classification methods are considered when user classes have many changes that lead to the creation of similar variable classes [12].

2.2.1.3 Classification of parallel networks

According to the spectral range of the sample classes selected on the image, the variance of the spectral values is calculated, in different bands used the minimum and maximum spectral values of the sample classes, quadrilaterals are created, which are called parallel networks. After creating parallel grids, the pixels of the image are classified depending on which of the four rectangles they are placed in, and they are divided into groups corresponding to the sample areas. The diameter of the error matrix shows the percentage of correctly classified classes and its other cells show the amount of commission error (row of each class in the error matrix) and emission error (column of each class in the error matrix). Kappa coefficient describes the degree of agreement between classification results and ground reality. Due to the fact that coincidental matches have occurred, they are removed from consideration [12].

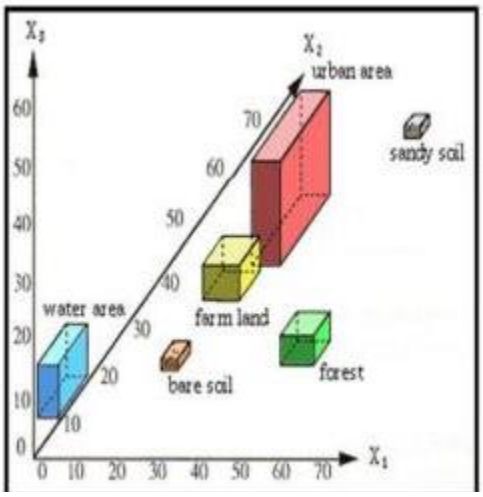

Fig. 4. Classification of parallel networks [12]

2.2.1.4. Maximum likelihood classification

One of the most accurate and widely used methods among the various supervised classification methods is the maximum likelihood method. This method evaluates the variance and covariance of different classes. It is assumed that all educational regions have a normal distribution function. After evaluating the probabilities in each class, the pixels are assigned to the classes that have the most similarity, and if the probability values are lower than the threshold, they introduce as unclassified pixel [17].

2.2.1.5. Decision tree algorithm

In each step, a dataset recognized and a branch is selected, then this branch is used to divide the dataset into subsets, and each subset is considered as a known dataset for the next step. The key to a decision tree algorithm is how to choose branches [13].

2.2.1.6 Random forest classification

There is a set of decision trees, each one gives a subset of data and their algorithms performs the learning operation. The random forest algorithm can select the class that has the most votes by voting and place it as the final class for the classification operation 15].

2.2.1.7 Support vector machines

Support vector machines (SVMs) [16] were originally designed for binary classification and are classifiers with a large boundary (edge) that try to separate different classes with a super-plane H having a maximum boundary. An important generalization of SVM is that the number of support vectors is very lower than the training samples in unlike other classifiers (such as decision trees).SVM provides the distances of each of the input support vectors from the optimal cloud plane [18].

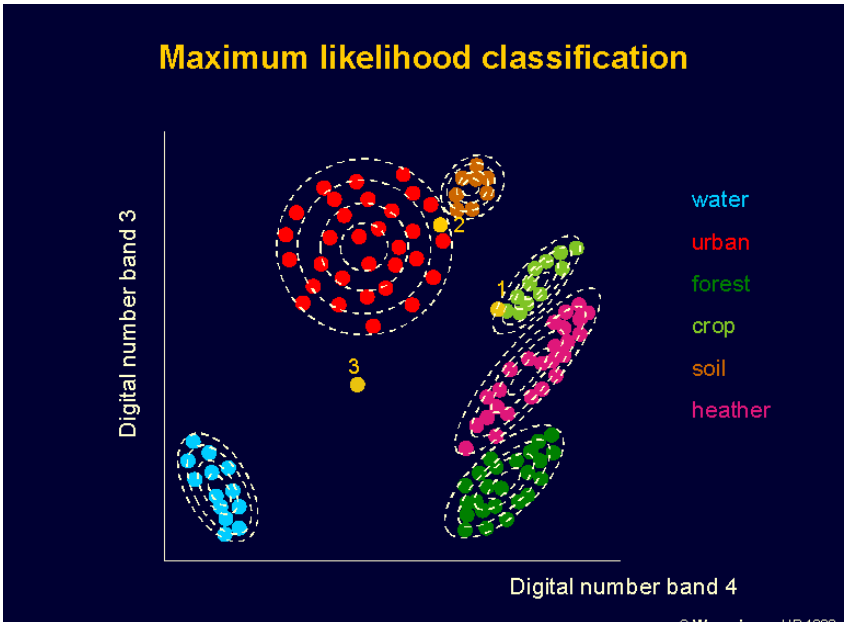

Fig. 5. Maximum likelihood classification [13]

Fig. 6. Decision tree classification [13]

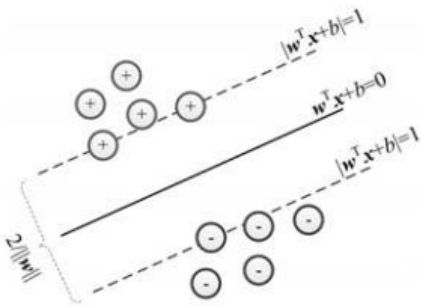

Fig. 7. A view of binary linear SV [15]

Binary linear SVM is the simplest, the training sample can be shown in the mathematical form x = {(xi,yi)} im =1; where in an input sample, m is the size of training samples, and a class label. 1 = yi if xi = C1 and -1 = yi if xi = C2. This problem can be converted into a parallel super-plane search problem as:

WTxi + b ≥ +1 for di = +1 (positive-plane)
WTxi + b ≤ -1 for di = -1 (negative-plane)

Where the vector W is the weight and b is the bias parameter [19] when data was potentially non-linear this method can't be used therefore a functions category, kernel functions (also called kernel) use for Correct separation of classes. The resulting feature space of kernel functions is called Reconstructive Hilbert Kernel Space (RKHS). An inner product in the RKHS space is equal to a mapping of the inner product of the samples in the original low-dimensional space. In other words,

K (xi , xj) = (Ø (xi), Ø(xj)) (1)

For all xi, where Ø is a mapping from the original feature space to a higher dimensional feature space and K is a kernel. Therefore, the kernel can simply replace the inner multiplication in the dual form of the optimization. According to the theory of Mercer [16], every positive semi-definite symmetric function is a kernel. Kernels are linear kernels.

$$K(x_i, x_j) = (x_i, x_j) \quad (2)$$

Polynomial kernel

$$K(x_i, x_j) = (x_i, x_j)^d \quad (3)$$

Where d is the polynomial degree, and Gaussian kernel (also called RBF kernel)

$$K(xi, xj) = \exp\left(\frac{|xi - xj|^2}{2Q^2}\right) \quad (4)$$

In fact, SVMS is a special kind of kernel method, that linear classifiers facilitated by the kernel trick [20]. Based on Fig. 8, by applying the kernel

function, samples that need non-linear classification can be easily separated with a page in the new space.

2.2.1.8 Neural network classification

This method follows the structure of the human brain and nerves [20]. It exists in several forms, the most common of which is the multi-layer perceptron [21]. A multi-layer perceptron usually consists of an input layer, one or more hidden layers, and an output layer, which respectively receives and processes information and then displays it [20]. Neural networks can be divided into two groups of feed-forward networks and divided returns.

2.2.2 Unsupervised classification methods

In unsupervised methods, spectral grouping is calculated automatically and only based on the mathematical difference of spectral values. Usually, this classification is used when the user does not have any information about the condition of the studied area.

2.2.2.1 k-means classification

Number of points in space must create in the K-Means algorithm. The number of these points should be the number of clusters that want to reach in the end, now calculate the distance of each of the samples with these points. After calculating the distance, each sample is assigned to the closest point category. Algorithm should be repeated several times until we reach a convergence, by moving other points, there will be no change in the average distance of the samples from the desired points.

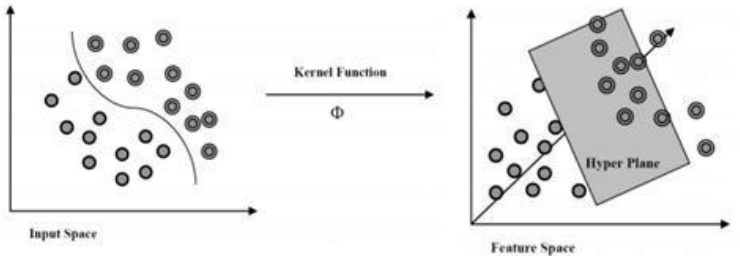

Fig. 8. Nonlinear separation using fan kernel SVMs [18]

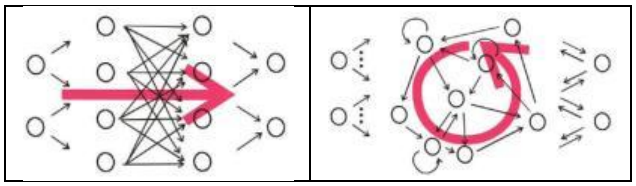

Fig. 9. The left side is a representation of the forward architecture, the right side is the return architecture [20]

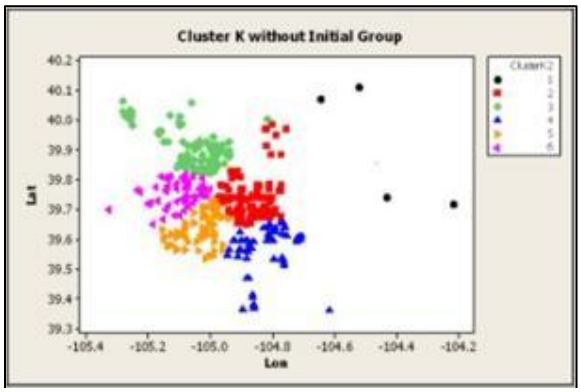

Fig. 10. k-means category [13]

2.2.2.2 Classification of ISO data

The Iso-data algorithm is similar to the k-means algorithm, with the difference that the Iso-data algorithm provides different numbers of clusters, while the k-means assumes that the number of clusters is known a priori.

2.2.2.3 Object oriented classification

This process is called multi-resolution segmentation, homogeneous objects by grouping pixels. Images can be classified based on texture, content, and geometric shape. Object-oriented classification can use multiple bands for classification [20].

2.3 Vegetation Indices

2.3.1 NDVI (Normalized Deference Vegetation Index)

The first and most famous index used to identify vegetation in remote sensing is the NDVI vegetation index and the most widely used vegetation index.

$$\mathrm{NDVI} = \frac{\mathrm{NIR+RED}}{\mathrm{NIR-RED}} \quad (4)$$

That NIR is near infrared band and RED is the red band values. This index has values between +1 and -1. The usual range of changes in green vegetation is equal to 0.2 to 0.8 the value of NDVI index is usually between 0.05 and 0.1 for sparse vegetation areas, and between 0.1 and 0.6 for normal and semi-dense vegetation areas. And for very dense plant areas, it is between 0.6 and 0.7 [22].

2.3.2 LAI (Leaf Area index)

The index is designed to estimate the density and volume of plants. The values of this index are from 0 to 3 and slightly higher. As the value of this index increases, it indicates an increase in the amount of vegetation in the studied area. This index has a positive and strong correlation with NDVI. In general, this index is used to estimate the density of vegetation along with predicting the growth rate in the study area.

$$LAI = (3.618 * EVI - 0.118) > 0 \quad (5)$$

2.3.3 VCI (Vegetation Condition Index)

VCI is the Vegetation Condition Index, The amount of vegetation on the surface of the earth is basically determined by the main of the environmental Physical components such as climate and soil are controlled. Purpose of VCI is identifying the effects of ecosystem change on vegetation in the region [22].

$$\mathrm{VCI} = \frac{\mathrm{NDVI-NDVI_{MIN}}}{\mathrm{NDVI_{MAX}-NDVI_{MIN}}} \quad (6)$$

2.3.4 SAVI (Soil Adjusted Vegetation Index)

The SAVI index is used to calculate the vegetation cover of the earth's surface, which has moderated the effect of the soil in it. This index is very little different from the NDVI vegetation index. To calculate this index, the following relationship is used:

$$SAVI = \frac{(1+L)(NIR-Red)}{(NIR+Red+L)} \quad (7)$$

L is the correction factor for soil background effects and varies from zero for denser vegetation to 1 for lower densities [23].

2.3.5 EVI (Enhanced Vegetation Index)

In this index, atmospheric scattering effects are removed or adjusted in terms of electromagnetic scattering. This index is very suitable for justifying the relationship between NDVI and LAI. In this spectral index, the blue band is used to correct the effect of background soil signals and atmospheric scattering. The most important application of this index is in the calculation of leaf area index (LAI). This index is calculated from the following relationship.

$$EVI = 2.5 * \frac{(NIR-Red)}{(NIR+6*RED-7.5*Blue+L)} \quad (8)$$

2.4 Evaluation of Accuracy

The assessment of the accuracy for satellite images is actually the estimation of the difference between the classification done with the reference data. Error matrix compares the relationships between the data of a specific source with the results of automatic classification in a class-by-class manner [24]. The overall accuracy of land use maps for land resource management should be mostly 0.85 for the majority of classes [25].

2.4.1 Overall accuracy

The overall accuracy is obtained from the sum of the elements of the main diameter of the error

matrix divided by the total number of pixels, according to the equation below [26].

$$OA = \frac{1}{N} \sum P_{ii} \quad (9)$$

In this regard: OA = total accuracy, N = number of test pixels and $\sum P_{ii}$= the sum of elements of the main diameter of the error matrix.

2.4.2 General accuracy

By dividing the total number of correctly classified pixels by the total number of pixels under investigation, the overall accuracy is obtained [13].

2.4.3 User Accuracy

The user accuracy expresses the probability that a certain class on the ground is placed in the same class on the classified image as below:

$$\text{User accuracy} = \frac{c_{ii}}{c_i} \times 100\% \quad (10)$$

Where, c_{ii} is =element at position ath row and ath column and c_i=column sums and c_i = row sums.

2.4.4 Accuracy of production

The manufacturer's accuracy is obtained by dividing the number of pixels that are correctly classified in each class by the number of ground reality pixels (training sample) used in that class (column sum). This criterion expresses how well the ground reality (pixels of the training sample) are correctly classified [24].

2.4.5 Kappa coefficient

The kappa coefficient K is a second measure of classification accuracy which incorporates the off-diagonal element as well as diagonal term to give a more robust assessment of accuracy than overall accuracy it is computed as: [1]

$$k = \frac{\sum_{a=1}^{u} \frac{c_{aa}}{Q} - \sum_{a=1}^{U} \frac{c_a c_a}{Q^2}}{1 - \sum_{a=1}^{U} \frac{c_a c_a}{Q^2}} \quad (11)$$

Where c_a =row sums.

3. RESULTS AND DISCUSSION

As a result, to monitor land use changes, the area of Behesht Zahra lands and waste disposal and recycling of Kahrizak waste has been removed from the landfill. These two ranges are examined separately at the end. In the figure, the boundaries of Behesht Zahra lands and the waste disposal and recycling of Kehrizak along with a buffer of 10 km from the landfill center are shown on the Landsat image dated 2022/05/25. In the southwestern part of the studied area, Feshafuye artificial lake can be seen. This artificial lake with an area of almost 7 hectares was built in 2015.

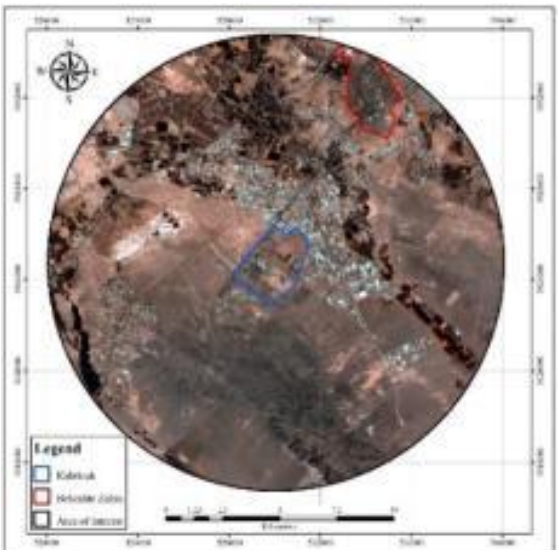

Fig. 11. Showing the scope of Behesht Zahra lands and Kahrizak waste disposal on the picture 2022/05/25

The training and test data were selected with the same distribution in the entire image to make the classification more accurate and to minimize the error. For this research, 4 classes of building, soil, water and agricultural land have been selected.

Building (urban area) class is shown in red, soil in yellow, water in blue and agricultural land in green. Classifications were done using training samples and the classifications were evaluated using test samples. The classifications performed on the Landsat image dated 25/09/2022 using training data (Fig. 12) and the overall accuracy and Kappa coefficient are calculated using test data (Fig. 13).

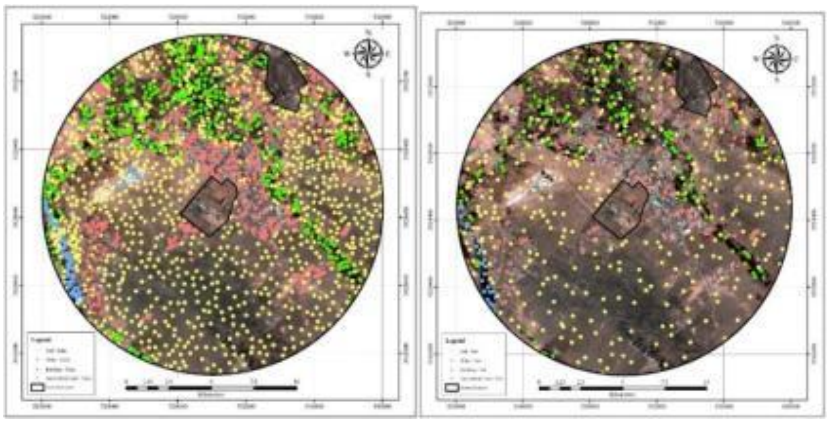

Fig. 12. Dispersion of training samples

Fig. 13. Dispersion of test samples

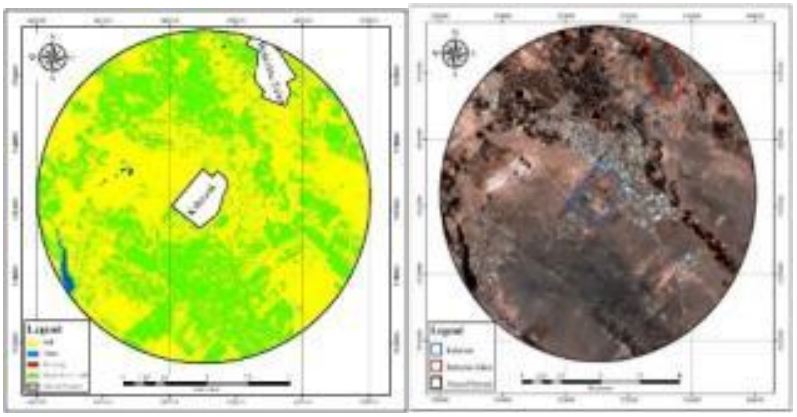

Fig. 14. Classification of parallel networks

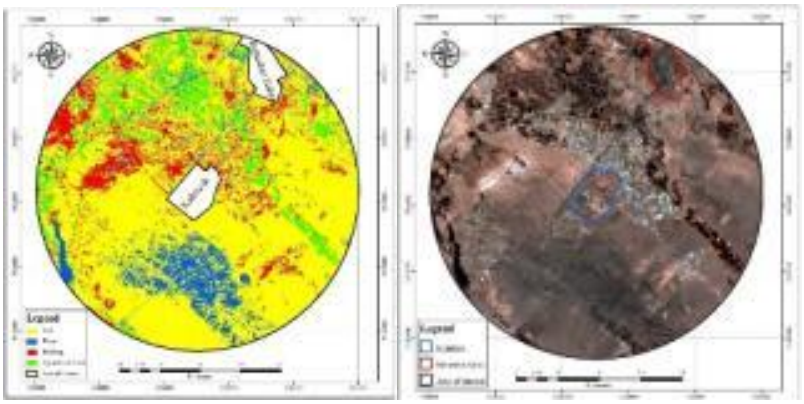

Fig. 15. Classification of the minimum distance from the mean

In the figures above, the classification method of parallel networks for the studied area has an overall accuracy (45.4962%) kappa coefficient (0.2897) that these are very low and is not appropriate. The classification method of the minimum distance from the average compared to parallel networks has a higher overall accuracy (75.2672%) and kappa coefficient (0.6134**)**, this method could not classify the satellite image well, neither.

The neural network classification method has higher overall accuracy (81.5267%) and kappa coefficient (0.7253) than the parallel and minimum distance network classification methods, but a lot of error is observed in the classified image and is not available in the original image, as a result, this classification method is not approved. Mahalanobis distance method has better overall accuracy (85.0382%), kappa coefficient (0.7657) and visual results than the minimum distance, but a large error is also observed in the above classified image.

The support vector machine circular kernel classification method is one of the best classification methods, this method has overall accuracy (89.0076%), kappa coefficient (0.8244) and acceptable visual results.

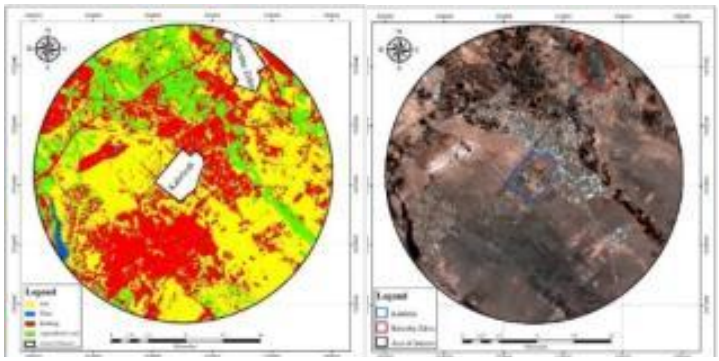

Fig. 16. Neural network classification

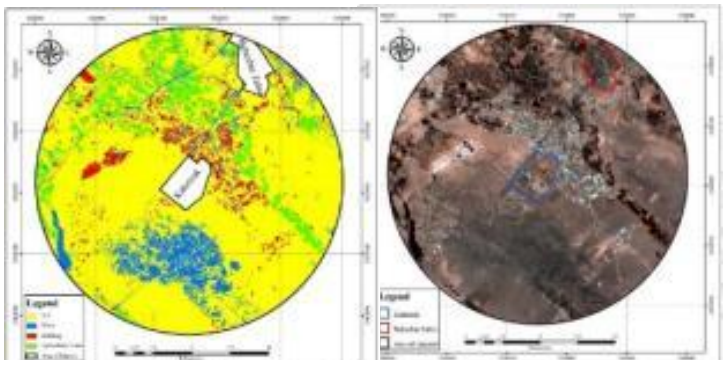

Fig. 17. Mahalanobis distance classification

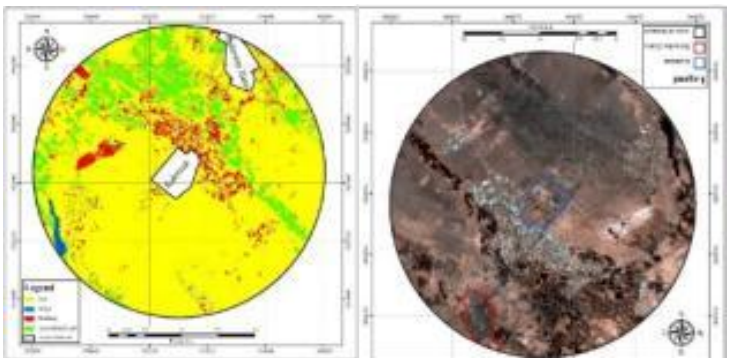

Fig. 18. Support vector machine classification with circular kernel

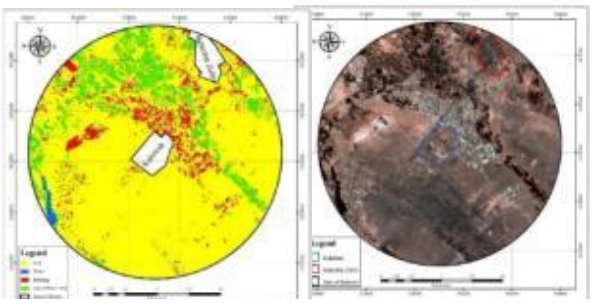

Fig. 19. Support vector machine classification with radial kernel

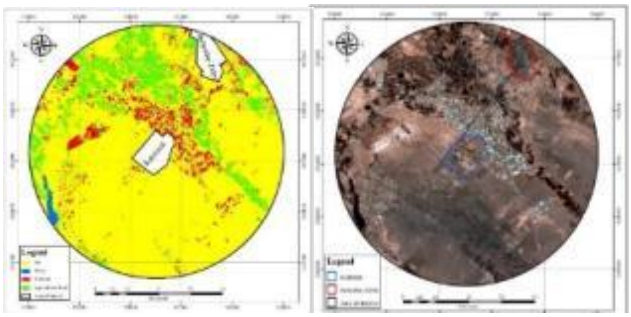

Fig. 20. Support vector machine classification with polynomial kernel

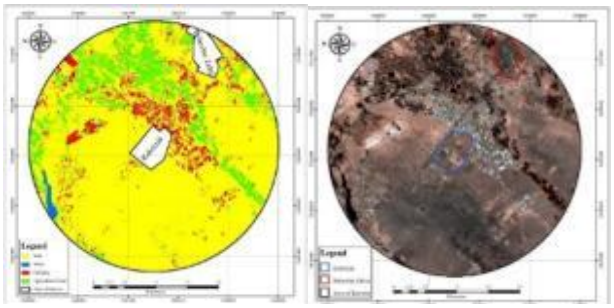

Fig. 21. Support vector machine classification with linear kernel

For this study area the circular kernel has a lower overall accuracy and kappa coefficient than other kernels. Support vector machine classification method with radial kernel has the same overall accuracy (89.0076%) and kappa coefficient (0.8246**)** with circular kernel, which shows the power of this classification method.

Support vector machine classification with polynomial kernel has overall accuracy (89.1603%) and kappa coefficient (0.8272**)** slightly higher than two circular and radial kernels, but visually, this method has also performed complication classification with higher accuracy. on the other hand linear kernel method has higher overall accuracy (89.6183%) and kappa coefficient (0.8346**)** than the other three kernels. By observing the results of overall accuracy and kappa coefficient calculated from four kernels, we can conclude that the support vector machine classification with all four kernels have acceptable results.

By comparing the overall accuracy (90.9924%), kappa coefficient (0.8591) and visual results of the performed classifications, it can be concluded that the maximum likelihood classification method has the best results compare to other classifications and is more suitable for the study area. In the next step, the mentioned indices are calculated and the best classification method or vegetation index is selected by comparing the two parameters of kappa coefficient and overall accuracy and visual observation of the results. Next, the results of five well-known and widely used vegetation indices NDVI, EVI, SAVI, LAI and VCI are shown and the results of the vegetation index are evaluated using test data.

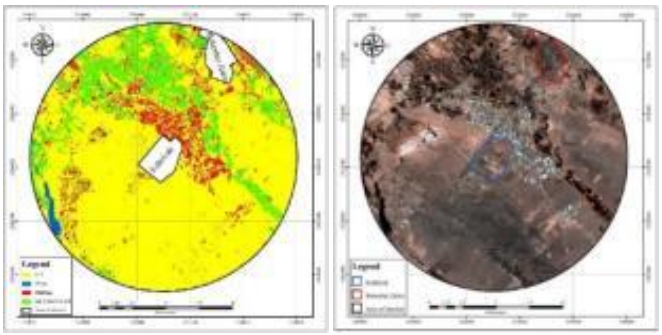

Fig. 22. Maximum likelihood classification

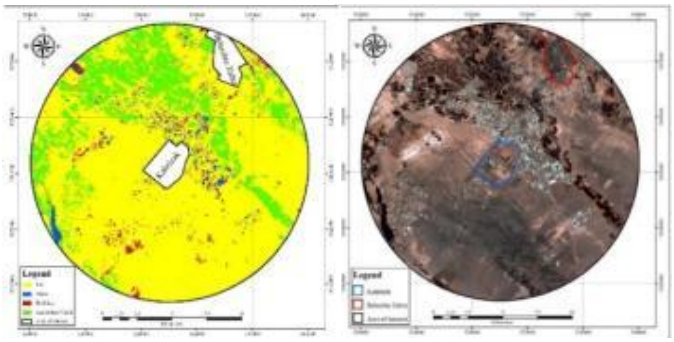

Fig. 23. LAI index

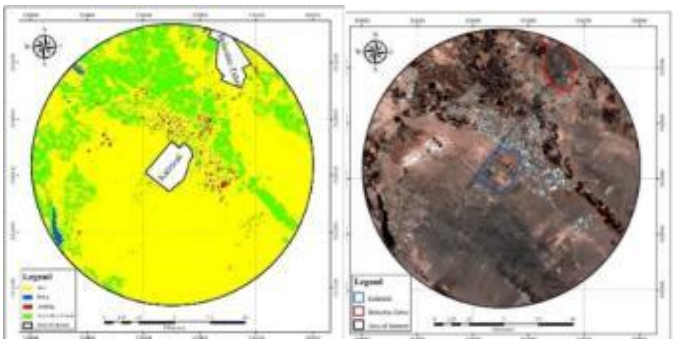

Fig. 24. SAVI index

The leaf area index is designed to estimate the density and volume of the plant. In the above figure it is obvious that this method does not separate the construction and water areas well and has a low overall accuracy (69.3129%) and kappa coefficient (0.5648**)**. As a result, this index cannot be used for further research. The adjusted plant index for soil has better overall accuracy (70.2290%) and kappa coefficient (0.5723) than the leaf area index, but this index also could not separate the construction and water areas well.

According to the figure overall accuracy for NDVI= 70.6870% and Kappa coefficient = 0.5760, the results of this index are similar to the previous two indices. The normalized difference index of vegetation cover is very suitable for separating soil areas from vegetation cover, but it doesn't work well for separating construction areas from water. The vegetation condition index is calculated from the normalized vegetation difference index, but for the studied area, it has shown better results than the NDVI with overall accuracy = 71.1450% Kappa Coefficient = 0.5798. This index, like other indices, has performed poorly in separating construction areas from water.

The highlighted vegetation index is actually the normalized vegetation difference index that has been optimized. This index has a better

evaluation result than other indices with overall accuracy = 71.2977% and kappa coefficient = 0.5810. As a result, the vegetation indicators for the study area of this research, which has 4 classes of water, soil, building and vegetation, have not been evaluated visually .Among the classification methods, maximum likelihood with overall accuracy of 90.99% and kappa coefficient of 0.85 was chosen as the best method. Among the vegetation indices, the highlighted vegetation index (EVI) was selected as the best index with an overall accuracy of 71.29% and a Kappa coefficient of 0.58. In the next step, by implementing the maximum likelihood classification method on all the satellite images obtained for this study and producing land use maps for each year and calculating the area of classes, it is possible to examine the trend of land use changes in the Kahrizak waste center in the last 10 years.

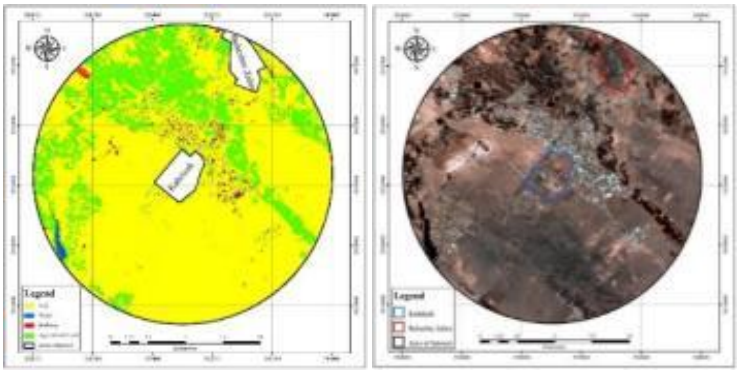

Fig. 25. NDVI index

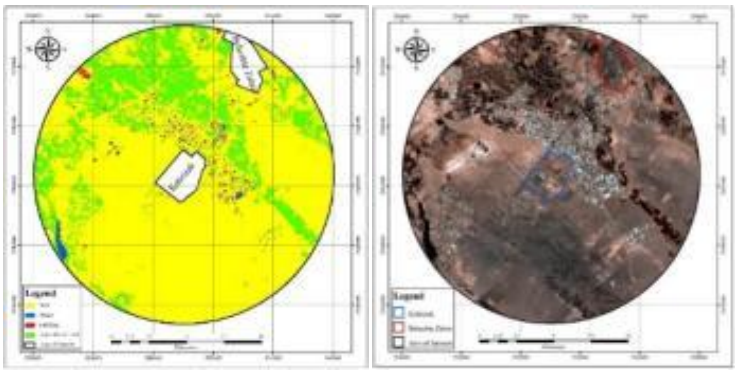

Fig. 26. VCI index

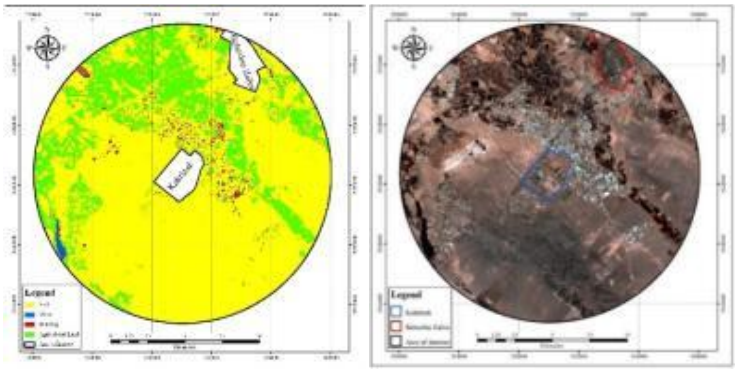

Fig. 27. EVI index

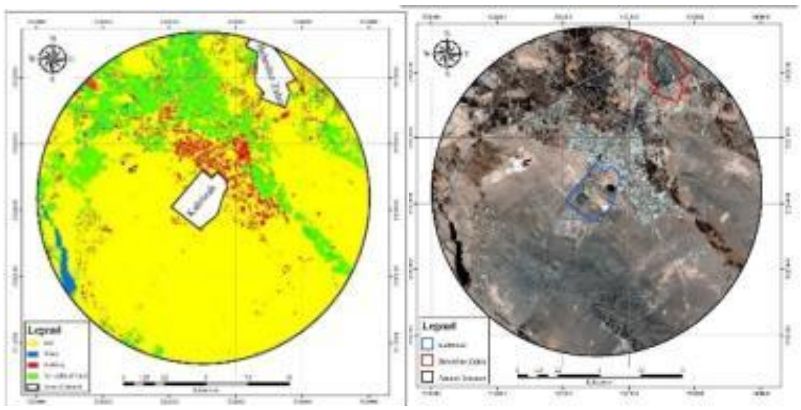

Fig. 28. Maximum likelihood classification on the 2013

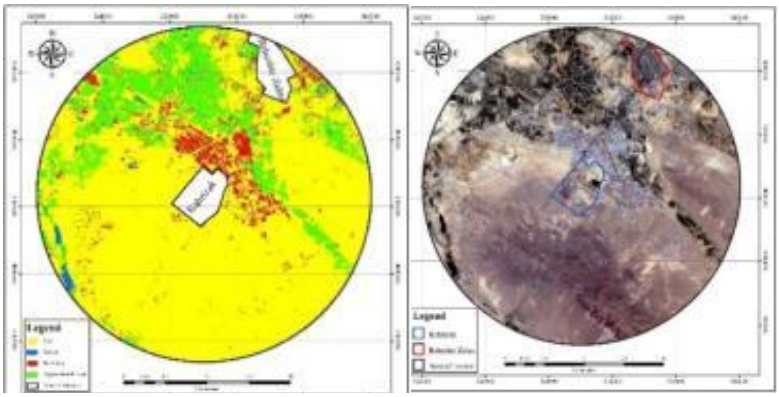

Fig. 29. Maximum likelihood classification on the 2014

By performing the maximum likelihood classification with overall accuracy = 90.4419**%** & Kappa Coefficient = 0.7792 method for image dated 2013/09/16, the area of the classified water class in the image, the part which is related to the Fashafuye artificial lake, is 4.38975 square kilometers, buildings are 15.4035 square kilometers, agricultural lands. 51.319575 square kilometers and the rest of the area under study, which consists of soil class, is equal to 229.30515 square kilometers. 3milion fish in the lake died due to sewage entering the lake water in2014. This news was not only very important from the point of view of the environment, but also questioned the health issues of the region. As a result, in the Landsat image taken on 2014/09/19 the water of lake is very low, which indicates that the lake's dirty water has been replaced. In the classification done on this image with Overall Accuracy = 91.3705**%** & Kappa Coefficient = 0.7872, the area of water class is 2.8053 square kilometers, building is 16.59285 square kilometers, agricultural land is 46.655325 square kilometers and soil class is 234.3645 square kilometers. Due to the very low amount of rain in 2013, the area of agricultural land has decreased compared to the previous year and the area of the soil class has increased, and building (urban area) is increased too.

In the classification done on the Landsat image by overall accuracy = 93.9096**%** & Kappa Coefficient = 0.8090 on 2015/09/06, the area of water class is 3.568725 square kilometers, buildings are 16.610625 square kilometers, agricultural lands are 49.77405 square kilometers, and soil class is 230.464575 square kilometers. The results show that the area of water class, building and agricultural land has increased compared to 2013.With the classification done on the Landsat image with overall accuracy = 93.6148**%**& kappa coefficient = 0.7806, dated 2016/08/23, the area of water class is 2.9016 square kilometers, building is 21.01275 square kilometers, agricultural land is 49.281075 square kilometers and soil class is 227.22255 square kilometers. The area of the building class has increased by 0.26% compared to the previous year and agricultural land has decreased by 1%.

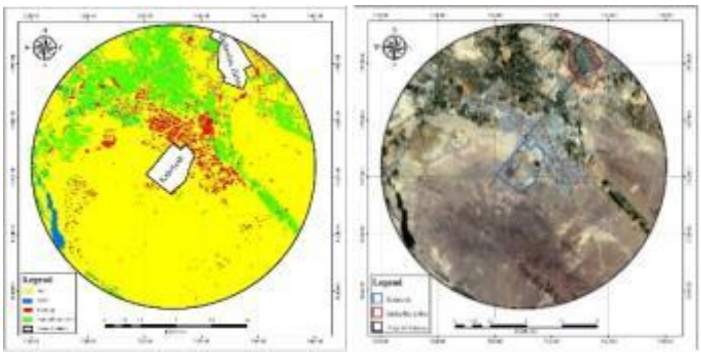

Fig. 30. Maximum likelihood classification on the 2015

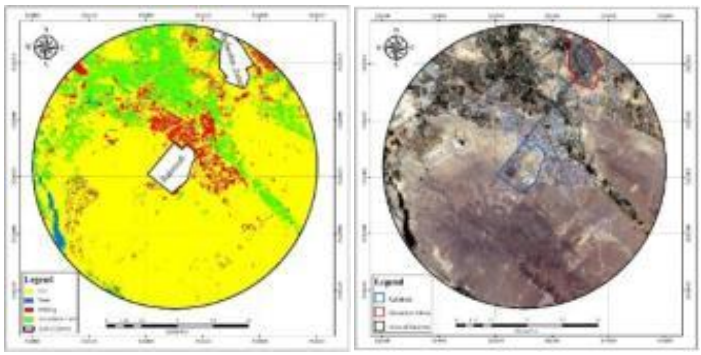

Fig. 31. Maximum likelihood classification on the 2016

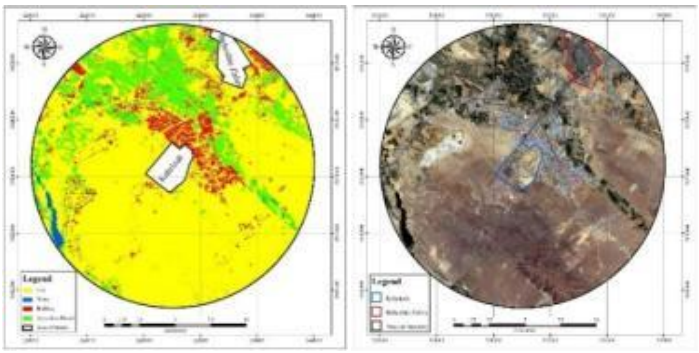

Fig. 32. Maximum likelihood classification on the 2017

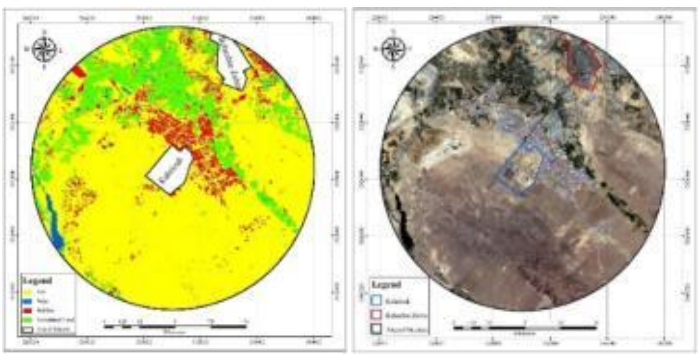

Fig. 33. Maximum likelihood classification on the 2018

With the classification done on the Landsat image with Overall Accuracy = 90.5749**%** & Kappa Coefficient = 0.7803, dated 09/11/2017, the area of water class is 2.8296 square kilometers, building is 21.216375 square kilometers, agricultural land is 49.4073 square kilometers and soil class is 226.9647 square kilometers. The area of the building class has increased by 0.2 and agricultural land by 0.12 square kilometers compared to the previous year. In the classification of the image with Overall Accuracy = 90.4067**%** & Kappa Coefficient = 0.8481, dated 2018/09/14, the area of water class is 2.95335 square kilometers, building is 22.578525 square kilometers, agricultural land is 48.18015 square kilometers and soil class is 226.70595 square kilometers. The area of the building class has increased by 1.36 square kilometers compared to the previous year, and the agricultural land has decreased by 1.22 square kilometers.

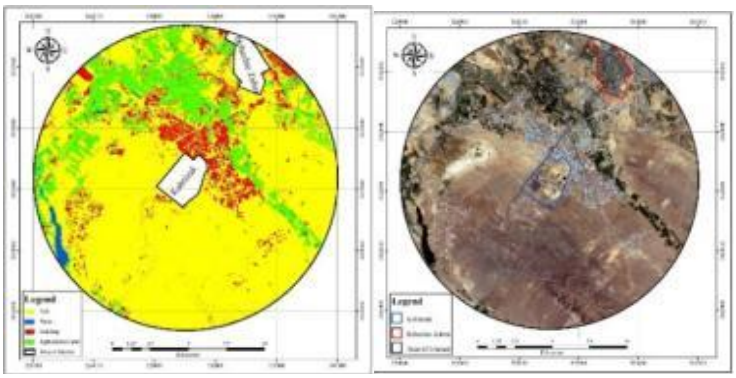

Fig. 34. Maximum likelihood classification on the 2019

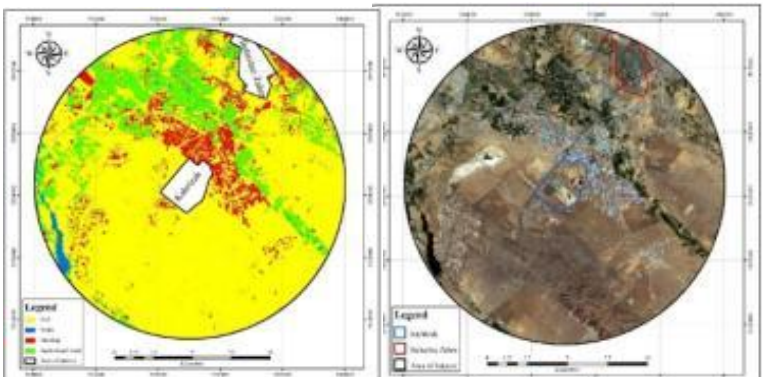

Fig. 35. Maximum likelihood classification on the 2020

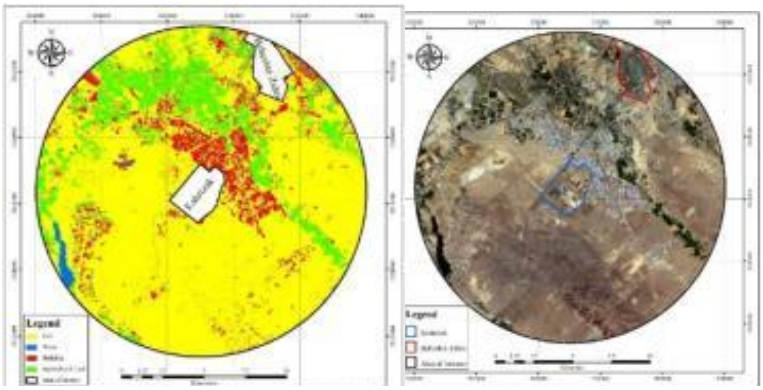

Fig. 36. Maximum likelihood classification on the 2021

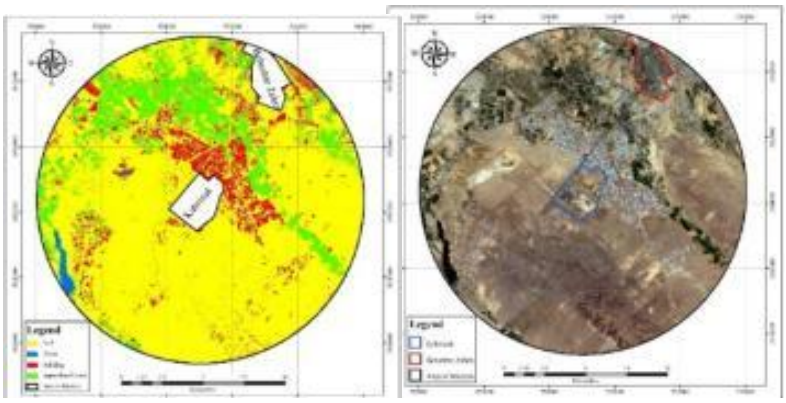

Fig. 37. Maximum likelihood classification on the 2022

Table 1. Area of classified classes in 10 years

Year/Class	Water km^2	Building km^2	Agricultural lands km^2	Soil km^2	Sum km^2
2013	4.38975	15.4035	51.319575	229.30515	300.417975
2014	2.8053	16.59285	46.655325	234.3645	300.417975
2015	3.568725	16.610625	49.77405	230.464575	300.417975
2016	2.9016	21.01275	49.281075	227.22255	300.417975
2017	2.8296	21.216375	49.4073	226.9647	300.417975
2018	2.95335	22.578525	48.18015	226.70595	300.417975
2019	2.722725	25.547625	46.5795	225.568125	300.417975
2020	2.6091	25.5467	44.644725	227.63745	300.437975
2021	2.000025	26.276625	41.689575	230.45175	300.417975
2022	2.9313	26.3502	41.301125	229.83535	300.417975

In the classification with Overall Accuracy = 90.8818**%** & Kappa Coefficient = 0.8560 dated 09/17/2019, the area of water class is 2.722725 square kilometers, building is 25.547625 square kilometers, agricultural land is 46.5795 square kilometers and soil class is 225.568125 square kilometers. The area of the building class has increased by 2.96 square kilometers compared to the previous year, and agricultural land has decreased by 1.6 square kilometers. According to Fig. 35 with Overall Accuracy = 93.0685**%** & Kappa Coefficient = 0.8278 dated 2020/09/19, corresponding to 2019/06/29, the area of water class is 2.6091 square kilometers, building is 25.5467 square kilometers, agricultural land is 44.644725 square kilometers and soil class is 227.63745 square kilometers. The area of the building class has not changed compared to the previous year, but the agricultural land has decreased by 1.93 square kilometers.

On 2021/09/22 by Overall Accuracy = 90.2813**%** & Kappa Coefficient = 0.8343 in classification, the area of water class is 2.000025 square kilometers, building is 26.276625 square kilometers, agricultural land is 41.689575 square kilometers and soil class is 230.45175 square kilometers. The area of the building class has increased by 0.73 square kilometers compared to the previous year, and agricultural land has decreased by 1.93 square kilometers. By applying classification to 2022/09/25 with Overall Accuracy = 90.9924**%** & Kappa Coefficient = 0.8591, the area of water class is 2.9313 square kilometers, building is 26.3502 square kilometers, agricultural land is 41.301125 square kilometers and soil class is 229.83535 square kilometers. The area of the building class has increased by 0.07 square kilometers compared to the previous year, and agricultural land has decreased by 0.38 square kilometers. In the table below, the area of the classified classes in 10 years is calculated in square kilometers .It is clear that the area of the building class (urban area) has increased and the agricultural land class has decreased. The building class has increased by 71% or 10.9467 square kilometers in ten years. The class of agricultural lands has decreased by 80% in the period studied by this

research, equivalent to 10.01845 square kilometers.

In the graphs below, the process of changes can be better analyzed. The most important changes are observed in the class of buildings and agricultural lands. To clarifying the below graph, the increase in the building class is directly related to the decrease in the agricultural land class. On the other hand, by observing this process of changes, it is possible to predict what changes will be made in the amount of construction and agricultural land in the region in the next few years.

The water class has also been added in the diagram below, but as mentioned, most of the area of the classified water class in the image related to the Fashafoye artificial lake is exposed, and this artificial lake is always full of water. Only in 2014, they had to change the water in the lake, and these changes can also be seen in a very detailed diagram.

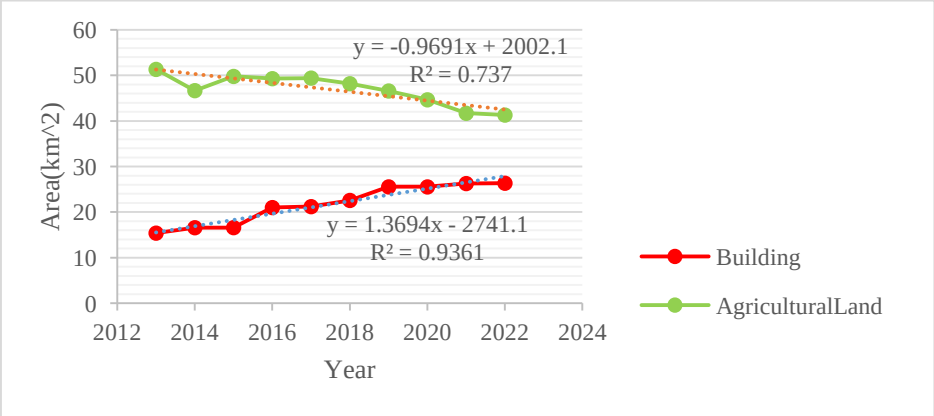

Chart 1. Comparison of changes in building class and agricultural land

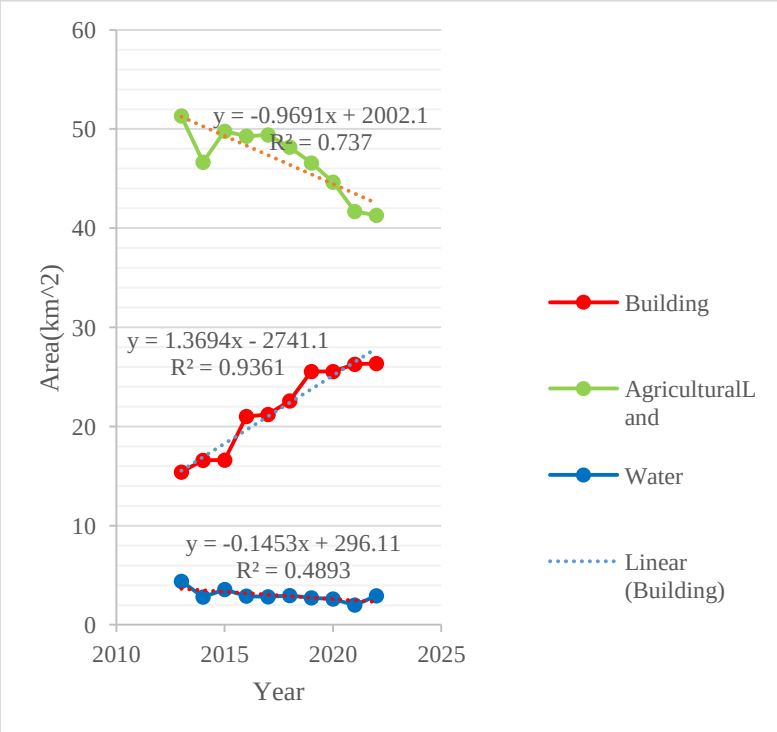

Chart 2. Comparison of changes in building class, agricultural land and water

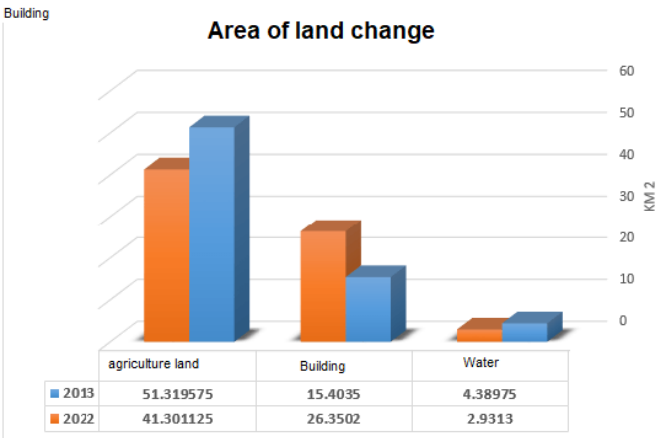

Chart 3. Comparison of changes in building class, agricultural land and water

In the following, the changes of the two areas of Behesht Zahra and the waste disposal and recycling of Kahrizak have been investigated. The spatial resolution of Landsat images is 15 meters, so it assume that they are not suitable for observing the effects in precise detail, therefore, visual observation of Google Earth images with the same date of Landsat images has been used to check the changes of the waste disposal and recycling center in Kahrizak. Google Earth images are updated using commercial Airbus images that have a spatial resolution of 30 to 50 cm. Landsat and Google Earth images of Kahrizak waste disposal and recycling center are shown in the figure.

The recycling center of Kohrizk, which was considered for landfill in 1956, was more than 15 kilometers away from the city limits of Tehran. Caused many problems, including water, soil and environment pollution in the region, which due to the south to north winds, the unpleasant smell of this center can be smelled even in the center of the capital. Kehrizak (Arad Koh) landfill center, which initially started with an area of 350 hectares, today this area has increased to nearly 1000 hectares. And at the same time, in terms of burying, several artificial hills have been created to bury garbage, which with a height of nearly 60 meters from the ground surface has caused the creation of water lakes, which has caused pollution and unpleasant odors, as well as many environmental problems. Google Earth images along with Landsat images were used to investigate the area of Behesht Zahra lands as well as the area of waste disposal and recycling in Kahrizak. Landsat and Google Earth images of Behesht Zahra fields are shown in the Fig. 39.

2013-09-16
Landsat8 image

2013-10
Google earth image

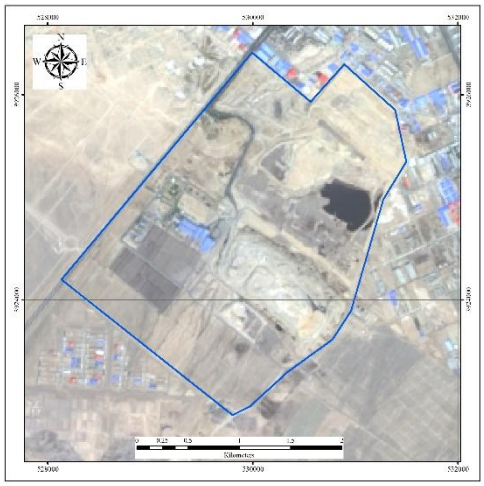

2014-09-19
Landsat8 image

2014-10
Google earth image

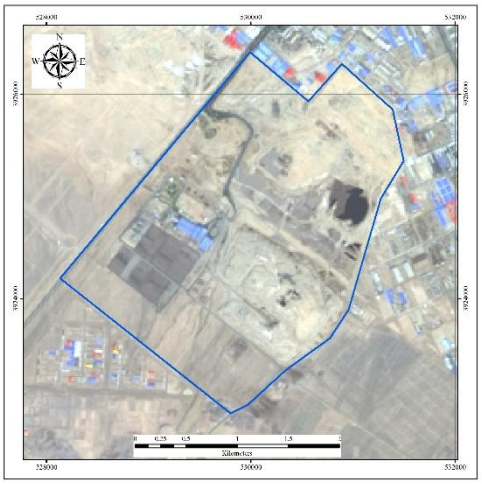

2015-09-06
Landsat8 image

2015-09
Google earth image

2016-08-23
Landsat8 image

2016-08
Google earth image

2017-09-11
Landsat8 image

2017-09
Google earth image

2018-09-14
Landsat8 image

2018-09
Google earth image

2019-09-17
Landsat8 image

2019-09
Google earth image

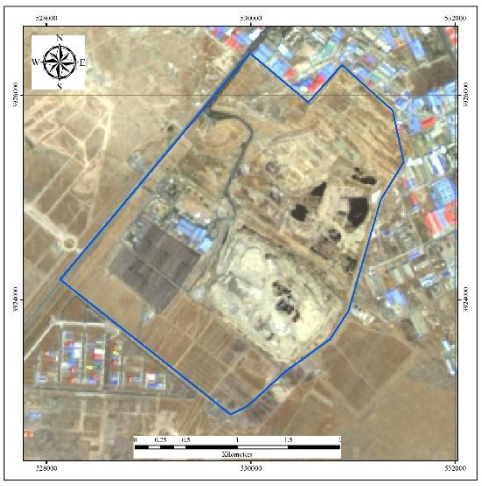

2020-09-19
Landsat8 image

2020-09
Google earth image

2021-09-22
Landsat8 image

2021-09
Google earth image

2022-09-25
Landsat8 image

2022-09
Google earth image

Fig. 38. Google Earth and Landsat satellite images of Kahrizak waste disposal and recycling center

جدول 1-**Error! No text of specified style in document.**

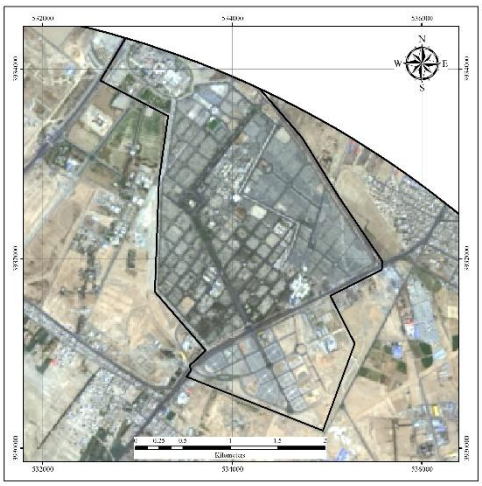

2013-09-16
Landsat8 image

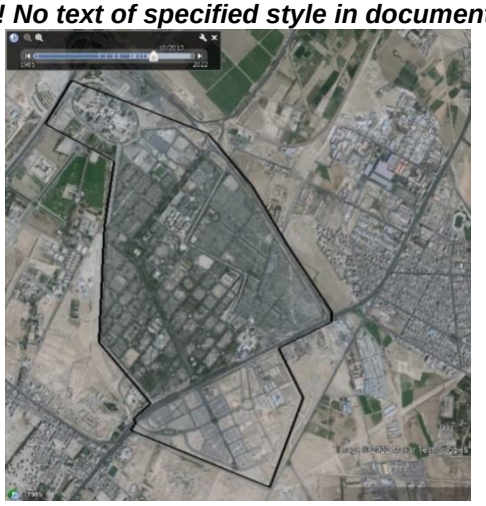

2013-10
Google earth image

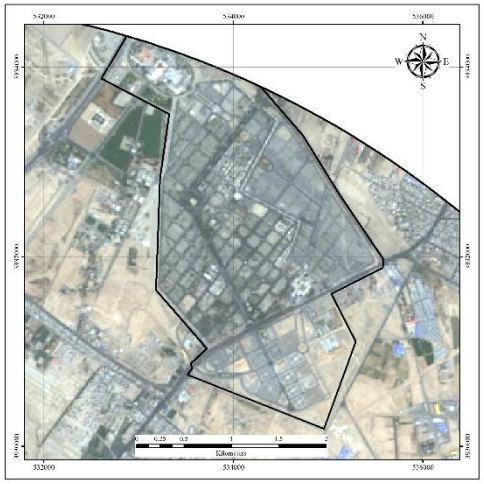

2014-09-19
Landsat8 image

2014-10
Google earth image

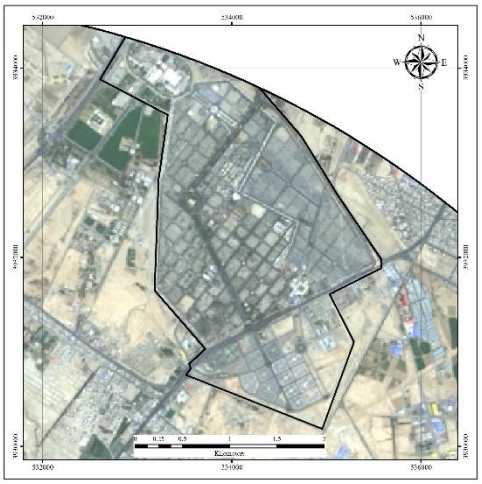

2015-09-06
Landsat8 image

2015-09
Google earth image

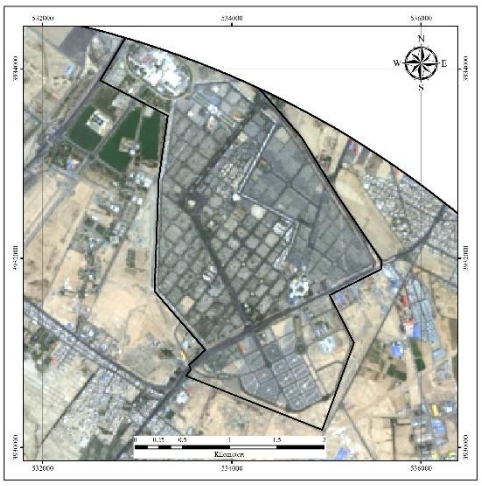

2016-08-23
Landsat8 image

2016-08
Google earth image

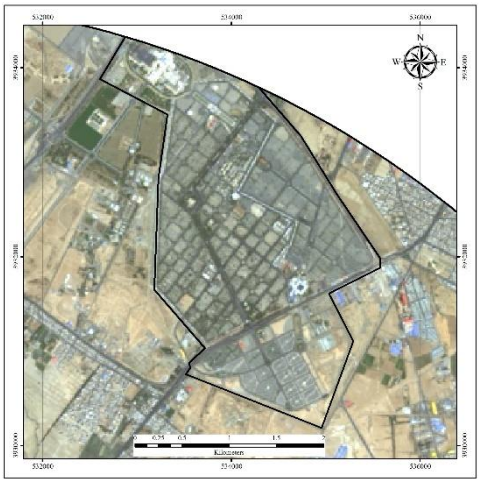

2017-09-11
Landsat8 image

2017-09
Google earth image

2018-09-14
Landsat8 image

2018-09
Google earth image

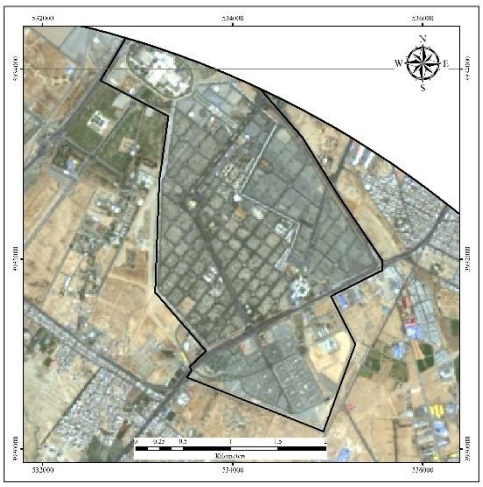

2019-09-17
Landsat8 image

2019-09
Google earth image

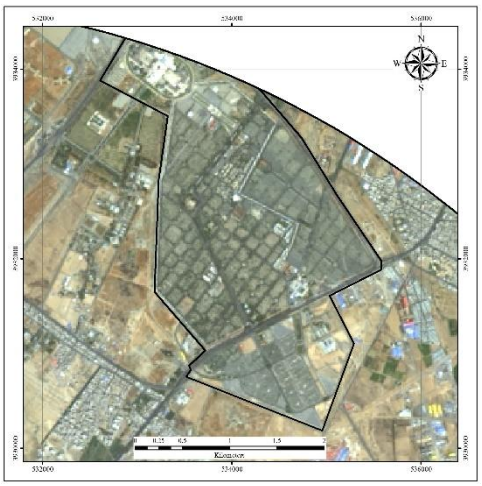

2020-09-19
Landsat8 image

2020-09
Google earth image

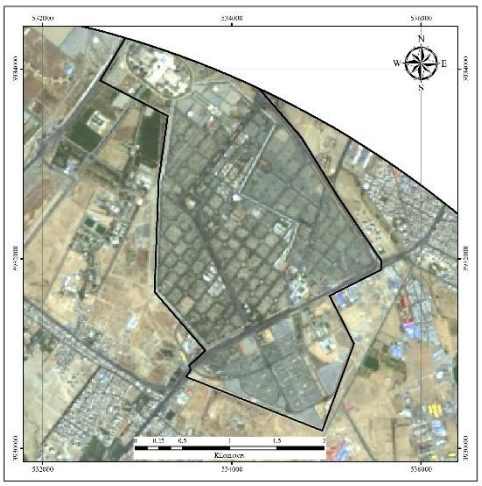

2021-09-22
Landsat8 image

2021-09
Google earth image

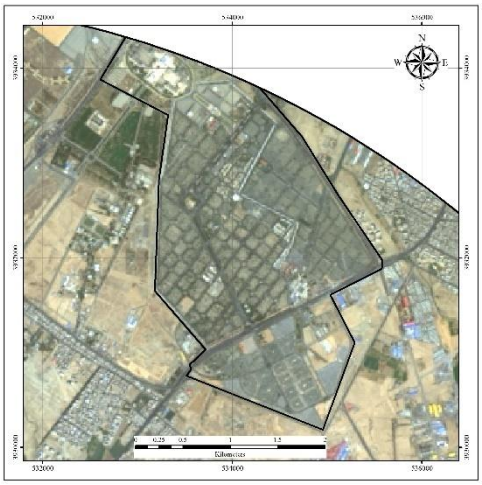

2022-09-25
Landsat8 image

2022-09
Google earth image

Fig. 39. Google Earth and Landsat satellite images of Behesht Zahra lands

Behesht Zahra was created with an area of 314 hectares, and the eastern side of Behesht Zahra used to be agricultural and livestock lands, which changed its use to a cemetery. Now, the cemetery has a total area of 584 hectares.

4. CONCLUSION

The purpose of this research is to monitor land use changes in the area of Kahrizak waste disposal center using remote sensing and spatial information system. In this research, it has been tried to select suitable images in terms of cloud cover and image quality from the month of September every year. Pre-processing has been done well on the images to increase the image quality. To choose the best method for producing a user map of five vegetation indices NDVI, EVI, SAVI, LAI and VCI and six supervised classification methods called maximum likelihood, parallel networks, minimum distance from the mean, neural network, Mahalanobis distance and support vector machines with Four circular, linear, polynomial and radial kernels with the same training and test data were evaluated on the image of 1401 using two parameters of overall accuracy and Kappa coefficient. For this research, four classes of soil, water, building and agricultural land have been selected. The results showed that the maximum likelihood classification method with overall accuracy of 90.99% and kappa coefficient of 0.85 and the high similarity of the classes of the generated land use map to the original satellite image was chosen as the best method. Then, a user map was generated from all the images from 1392 to 1401 using the maximum likelihood classification method. After calculating the area of the classes, the results showed that in the last decade, the area of the building class (the building class means roads and artificial constructions by humans) has increased by 71% In other words, an increase of 10.9467 square kilometers and the agricultural land class has decreased by 80% The equivalent of 10.01845 square kilometers.

5. FUTURE CHALLENGES

Based on what was obtained in this research, it is better to pay attention to the following things in future researches:

1- Images with higher spatial resolution should be used to classify images and produce user maps because spatial accuracy has a great impact on classification accuracy and complications with more details and smaller dimensions will be recognized.
2- - Creating an algorithm for identifying waste separation and washing centers that have caused the destruction of agricultural lands.

COMPETING INTERESTS

Authors have declared that no competing interests exist.

REFERENCES

1. Jensen J. Introductory digital image processing: A remote sensing perspective. Englewood Cliff, NJ: Prentice – Hall. 2005; 318.
2. AEa. SES. Monsef. Integrating remote sensing, geographic information system, and analytical hierarchy process for hazardous waste landfill site selection. Arabian Journal of Geosciences. 2019; 1-14.
3. SSA, GRK, MFA, JB. Detecting and assessing the spatial-temporal land use land cover changes of Bahrain Island during 1986–2020 Using Remote Sensing and GIS," Earth System and Environment, 2022.
4. Bea. Aslam. Identifying and ranking landfill sites for municipal solid waste management: An integrated remote sensing and GIS approach. Buildings. 2022; 605.
5. Aİea Karabulut. Landfill siting for municipal solid waste using remote sensing and geographic information system integrated analytic hierarchy process and simple additive weighting methods from the point of view of a fast-growing met. Environmental Science and Pllution Research. 2022; 4044-4061.
6. Norman L, Feller M, Guerin D. Forecasting urban growth across the United States-Mexico border. Compute. Environ. Urban Syst. 2009; 150-159.
7. NKTWN, Karimi AR. Development and application of an analytical framework for mapping probable illegal dumping sites using nighttime light imagery and various remote sensing indices. Waste Management. 2022; 143:195-205,.
8. IILO, Felix BJC. Locating suitable solid waste dumping sites using remote sensing and GIS Techniques in Aba Municipal, South-Eastern Nigeria. European Journal of Applied Sciences," Europen Journal of Applied SCIENCES. 2022; 10.2.
9. Surender Kumar RS. Geospatial applications in land use/land cover change detection for sustainable regional development: The Case of Central Haryana, India. GEOMATICS AND Environmental Engineering. 2021;15.
10. Guan Y, Zhou Y, He B, Liu X, Zhang H, Feng S. Improving land cover change detection and classification with BRDF correction and spatial feature extraction using landsat time series: A case of urbanization in Tianjin, China. IEEE J. Sel. Top. 2020; 4166-4177.
11. Seddiqi M. Investigating the changes in water basin of lakes by random forest classification method using Landsat images (Case study: Disturbed Lake). Master's thesis, Faculty of Technology and Engineering, Islamic Azad University (Tehran South Branch); 2018.
12. eaAlavi Panah,. Application of remote sensing in earth science (soil science). Tehran University Press; 2013.
13. Amin Ghasemi Esfahalan. Investigation of random forest method to improve the classification of urban land cover using satellite images, master's thesis. Faculty of Mapping Engineering, Khwaja Nasiruddin Toosi University; 2013.
14. Afshinfar A, et al. RS-based assessment: spatial-temporal changes in water basins of Tar and Havir Lakes. International Journal of Environment and Climate Change. March 2023; 13(5):159-178.
DOI:10.9734/ijecc/2023/v13i51757
15. Cristianini NaJST. An introduction to support vector machines and other kernel-based learning methods. Cambridge University Press; 2000.
16. Waske BaMB. Classifier ensembles for land cover mapping using multitemporal SAR imagery. ISPRS Journal of Photogrammetry and Remote Sensing. 2009; 450-457.
17. Vahidi et,al. Monitoring Land Cover Changes in Tehran City over 5 years (2018 to 2022) using Remote Sensing based Spatial Information,April 2023,Asian Journal of Environment & Ecology 20(3):24-35,DOI:10.9734/AJEE/2023/v20i3440
18. Burges CJ. A tutorial on support vector machines for pattern recognition. Data Mining and Knowleged Discovery. 1998; 121-167.
19. ZZH. In Ensemble methods: foundation and algorithms. CRC Press; 2012.
20. Dixon BaNC. Multispectral landuse classification using neural networks and support vector machines: one or the other, or both. International Journal of Remote Sensing. 2008; 1185-1206.
21. Richards J. Remote sensing digital image analysis: An introduction. Springer-Verlag, Berlin, Germany; 1999.

22. Bachmair S, Tanguy M, Hannaford J, Stahl K. How well do meteorological indicators represent agricultural and forest drought across Europe? Environ. Res. Lett. 2018; 34042.
23. Rezaei Moghadam MV. Modis data performance analysis in drought estimation.,Journal of Geography and Environmental Stability. 1991; 97-54.
24. TM. Lillesand R. Remote sensing and image interpretation. New York: John Wiley & Sons. Inc; 2001.
25. Re, Anderson. Metamorphic and basin fluids in quartz–carbonate–sulphide veins in the SW Scottish Highlands: a stable isotope and fluid inclusion study. Geofluids. 2004; 4.2:169-185.
26. SJ. Thematic validation of high-resolution global land-cover data sets. 1999; 1051-1060.
27. Bachmair S, Tanguy M, Hannaford J, Stahl K. How well do meteorological indicators represent agricultural and forest drought across Europe. 2018; 13: 34042.

Peer-review history:
The peer review history for this paper can be accessed here:
https://www.sdiarticle5.com/review-history/98767